Vortex magnetic domain state behavior in the Day plot

Wyn Williams[1], Roberto Moreno[1,2], Adrian R. Muxworthy[3,4], Greig A. Paterson[5], Lesleis Nagy[5], Lisa Tauxe[6], Ualisson Donardelli Bellon[7,1], Alison A. Cowan[3], Idenildo Ferreira [1]

[1]School of GeoSciences, University of Edinburgh, King's Buildings, West Mains Road, Edinburgh, UK.
[2]CONICET, Instituto de Física Enrique Gaviola (IFEG), Córdoba, Argentina
[3]Department of Earth Science and Engineering, Imperial College London, South Kensington Campus, London, UK.
[4]Department of Earth Sciences, University College London, London, UK.
[5]Department of Earth, Ocean and Ecological Sciences, University of Liverpool, Liverpool, UK.
[6]Scripps Institution of Oceanography, University of California San Diego, CA, USA.
[7]Department of Geophysics, Institute of Astronomy, Geophysics and Atmospheric Sciences (IAG), University of São Paulo, São Paulo, Brazil

Key Points:

- Vortex domain states for magnetite predominantly have pseudo-single-domain Day plot characteristics.
- If the mineralogy is known, the Day plot can provide an estimate on the dominance of stable remanence carriers.

Corresponding author: Wyn Williams, `wyn.williams@ed.ac.uk`

Abstract

The ability of rocks to hold a reliable record of the ancient geomagnetic field depends on the structure and stability of magnetic domain-states contained within the rock's magnetic particles. In paleomagnetic studies, the Day plot is an easily constructed graph of magnetic hysteresis parameters that is frequently used (and mis-used) to estimate the likely magnetic recording stability of samples. Often samples plot in the region of the Day plot attributed to so-called pseudo-single-domain (PSD) particles with little understanding of the implications for domain-states or recording fidelity. Here we use micromagnetic models to explore the hysteresis parameters of magnetite particles with idealized prolate and oblate truncated-octahedral geometries containing single domain (SD), single-vortex (SV) and occasionally multi-vortex (MV) states. We show that these domain states exhibit a well-defined trend in the Day plot that extends from the SD region well into the multi-domain (MD) region, all of which are likely to be stable remanence carriers. We suggest that although the interpretation of the Day plot and its variants might be subject to ambiguities, if the magnetic mineralogy is known, it can still provide some useful insights about paleomagnetic specimens' dominant domain state, average particle sizes and, consequently, their paleomagnetic stability.

Plain Language Summary

Ancient magnetic field recordings from rocks, provide information about the early habitability of Earth and formation of the Solar System. Key to understanding the reliability of these magnetic recordings is knowing the particle size of a rock's constituent magnetic minerals. Very small particles ($\lessapprox$100 nm) are magnetically uniform, but as the particle size increases the magnetic structures become non-uniform and increasingly complex. These different types of structures are termed domain states, and yield very different magnetic hysteresis responses, often summarized on a so-called "Day" diagram - a very commonly used diagnostic domain state (or particle size) plot. The position of particles in the size 100-1000 nm on the Day plot is poorly quantified. This is a problem, as it has been shown in the last five years, that this particle size range carries the most stable magnetic recordings, lasting potentially longer than the age of the universe. These particles contain vortex-like magnetic structures. Using a numerical micromagnetic algorithm, this is the first comprehensive study to quantify the magnetic response of vortex structures on the Day plot. We show that careful use of the Day plot provides insight into the ability of the sample to retain recordings of the ancient geomagnetic field.

1 Introduction

Knowing the domain state of the magnetic minerals contained within experimental samples is central to paleo- and environmental magnetism because the domain state informs us about both the particle size and importantly the magnetic recording fidelity of its paleomagnetic signal. The "Day plot" (Day et al., 1977) is a popular domain-state diagnostic plot derived from magnetic hysteresis and backfield-curve measurements. Day et al. (1977) has ∼3000 citations at the time of writing. The Day plot shows the ratios of the remanent saturation magnetization normalized by saturation magnetization ($M_{\mathrm{rs}}/M_{\mathrm{s}}$), versus the ratio of the remanent coercivity over coercivity ($B_{\mathrm{cr}}/B_{\mathrm{c}}$). The smallest particles, which are magnetically uniform and termed single domain (SD), have high $M_{\mathrm{rs}}/M_{\mathrm{s}}$ and low $B_{\mathrm{cr}}/B_{\mathrm{c}}$ and plot towards the upper left of the diagram. The largest particles (multidomain, MD) plot towards the lower right, and intermediate-sized particles (traditionally referred to as pseudo-SD, PSD), plot in the middle (Figure 1). Most published data fall within the PSD region of the Day plot, which has led several authors to criticize the use of such a plot to diagnose domain state (Tauxe et al., 2002; Roberts et al., 2018, 2019). This criticism is based partially on our general lack of understanding of what type of magnetic particles and phenomena contribute to the PSD region. Because magnetic hysteresis and backfield-curve measurements are performed on macroscopic bulk samples, the achieved magnetic parameters are a response to an assemblage of particles. These assemblages might not be uniform in terms of domain states. For example, they can be mixtures of pure SD and MD particles that might plot within the PSD region (as do vortex states) (Dunlop, 2002b). Furthermore, mixtures of SD and superparamagnetic particles (referred to as SP, a behaviour attributed to particles with instantaneous relaxation times) also plot within the PSD region (Tauxe et al., 1996). Despite the ambiguity in its interpretation, the Day plot remains popular partly because unlike other more complex domain state diagnostic tests (e.g., Roberts et al., 2000), its related data is relatively quick and easy to measure, it attempts to identify remanence rather than induced domain states, and it is also possible to summarize hundreds of different specimens on a single diagram.

The original domain state boundaries on the Day plot were based on a mixture of theory (Stoner & Wohlfarth, 1948) and experimental observations on synthetic (titano)magnetite samples. Notwithstanding some refinements (e.g., Dunlop, 2002a), the basic Day plot and its interpretation remain essentially the same. While it is possible to analytically calculate the behavior of SD particles controlled by various types of magnetic anisotropy, and also possible to experimentally determine Day plot parameters for very large, individual MD crystals, understanding the behavior in the paleomagnetically important high-remanence PSD range, i.e., 100 – 10,000 nm, has proven more challenging. There are two reasons

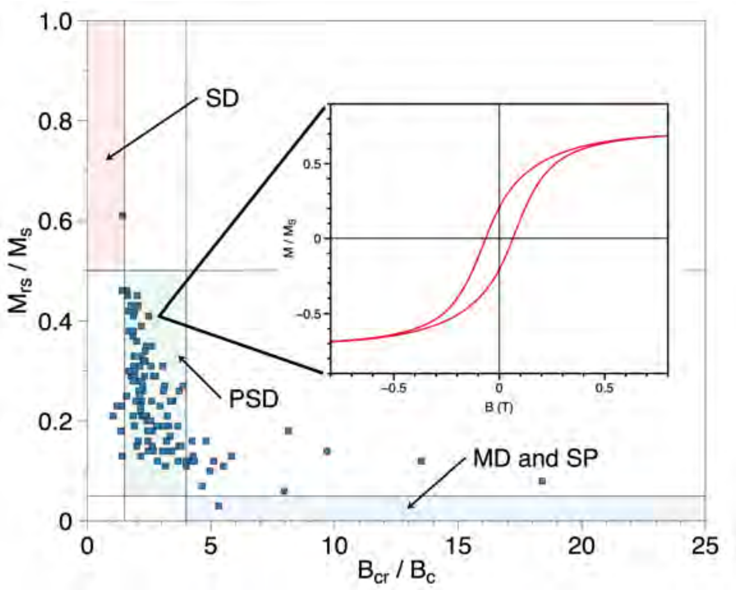

Figure 1. Hysteresis parameters from a collection of related specimens in a Day plot diagram, where the vertical axis is the remanence ratio ($M_{\mathrm{rs}}/M_{\mathrm{s}}$) and the horizontal one is the coercivity ratio ($B_{\mathrm{cr}}/B_{\mathrm{c}}$). The inset graph shows a typical loop from which the ratios were derived, where the red line is the measured loop corrected for para/diamagnetic contributions. The fields SD (single domain), PSD (pseudo-single domain), MD (multidomain) and SP (superparamagnetic) indicate the "usual" domain structure interpretation for the respective regions of the diagram.

for this: 1) production of non-interacting experimental samples with narrow particle-size distributions, which are also "stress-free" is challenging (King & Williams, 2000; Krása et al., 2011), and 2) the magnetic behavior of PSD particles is complex and theoretical models require numerical models (Brown, 1963).

Over the last 30 years, micromagnetics combined with nanometric magnetic imaging (Harrison et al., 2002; Almeida et al., 2014), has revolutionized our understanding of PSD particles. We now know that PSD particles are dominated by single-vortex (SV) and multi-vortex (MV) structures, which have been shown (Nagy et al., 2017; Nagy, Williams, Tauxe, Muxworthy, & Ferreira, 2019) to have magnetic stabilites equal to or exceeding that of SD particles and thus challenging the long-held view that SD particles carry the most stable paleomagnetic remanence (Néel, 1949). For many magnetic minerals, the particle size range for vortex states is predicted to be at least an order of magnitude greater than that of SD particles (Nagy et al., 2017) and thus there is an urgent need to be able to identify not only SD particles but also PSD/vortex behavior in the Day plot. In this paper, we follow Roberts et al. (2017) and refer to PSD signals as vortex signals for the rest of the paper, although SV particles are only one type of PSD domain structure.

1.1 How are vortex domain states represented on the Day plot?

There have been several previous attempts to characterize the vortex state contribution to the Day plot using micromagnetic numerical models. However, these are either older studies in which approximations were made and the models do not meet modern standards such as adequate model resolution or accounting for realistic particle morphologies (Williams & Dunlop, 1995; Tauxe et al., 2002; Muxworthy et al., 2003) or the Day plot was not the main focus and the results not comprehensive (Lascu et al., 2018; Valdez-Grijalva et al., 2018, 2020; Nikolaisen et al., 2020). Although not comprehensive, these studies have demonstrated that the Day plot is sensitive to both the particle size and morphology of vortex particles, and that particles just larger than the SD threshold size can plot very close to the MD region (Lascu et al., 2018; Valdez-Grijalva et al., 2018, 2020). Of particular note is the study of Nikolaisen et al. (2020), who examined a range of realistic particle sizes and shapes and reported predictions of SD and vortex states that are generally well grouped on the Day plot. These theoretical studies are supported by experiments on electron-beam lithography (EBL) samples of monodispersions of magnetite, which observe particles in the vortex domain state size range that plot at the PSD/MD boundary in the Day plot (Krása et al., 2011). EBL samples are arrays of nearly identical crystal, which is ideal for characterizing vortex behavior. However, the samples can suffer from stress induced by the coupling of the crystals with the thin-film substrate which, in turn, affects their Day plot characteristics.

Therefore, there is a need to determine the vortex state contribution to the frequently used Day plot. In order to fulfill such a task, in this paper, we have applied MERRILL (Conbhuí et al., 2018) to systematically determine the Day plot response for magnetite crystals as a function of both size and elongation. For that, we have used distributions of randomly orientated particles that simulate monodispersions that are capable of displaying both SD and vortex-state behaviors.

2 Methods

Our numerical models of Day plot hysteresis parameters were obtained using the open-source software package MERRILL, version 1.8.6p (Conbhuí et al., 2018; Williams et al., n.d.), which is a three-dimensional finite-element micromagnetic modeling application. While recognizing that the hysteresis parameters may be dependent on slight changes in particle morphology and surface irregularities, our aim is to examine the trends in hysteresis parameters as a function of particle size and idealised shape. We therefore consider truncated-octahedron shaped particles that were either elongated or compressed along the x-axis to create prolate or oblate particle morphologies. In some respects, this mirrors the standard single-domain analysis in ellipsoidal particles, but here we take a typical crystalline morphology and allow the magnetization to occupy non-uniform magnetic domain states and non-coherent domain switching mechanisms. MERRILL requires particle geometries to be defined in terms of a finite element mesh, and these were generated using the proprietary meshing package Coreform Trelis (Coreform LLC, 2017). In micromagnetic modeling it is important to have the maximum mesh size no greater than the material's exchange length l_{ex} (Rave et al., 1998), which for magnetite at 20 °C takes a value of 9 nm. l_{ex} is related to the width of transitions between domains, and if it is too large the inhomogeneously magnetized states will be poorly characterized. All our model geometries were meshed at a mean size of 8 nm.

All models were of stoichiometric magnetite at 20 °C defined in terms of the four temperature dependent material constants of saturation magnetization M_{S}, magnetocrystalline anisotropy constants K_1 and K_2, and the exchange constant A_{ex} which take the values of $4.825 \cdot 10^5$ A/m^3 (Pauthenet & Bochirol, 1951), $-1.304 \cdot 10^4$ J/m^3 and $-3.154 \cdot 10^3$ J/m^3 (Fletcher & O'Reilly, 1974) and $1.344 \cdot 10^{-11}$ J/m (Heider & Williams, 1988) respectively. It should be noted that the models presented here do not include thermal fluctuations, whose principle effect is to reduce the particles' remanent magnetization for weakly stable domain states. Such particles are also commonly referred to as superparamagnetic (SP) particles.

In all, a total of 556 models of prolate and oblate geometries were performed, covering a wide range of stable-single-domain (SSD, hereafter referred to as SD) and single-vortex (SV) domain states. The prolate geometries consist of 17 particle sizes from 40 to 200 nm in steps of 10 nm, and each size having elongations along $\langle 100 \rangle$ of axial ratios (AR, long axis/short axis) of 1.00 to 2.00 in 0.05 steps, 2.00 to 3.00 in 0.25 steps, and 3.00 to 5.00 in 1.00 steps. The oblate particles consist of 16 particle sizes from 45 to 195 nm in steps of 10 nm, and each size is compressed along $\langle 100 \rangle$ to AR's of 0.909, 0.500, 0.250 and 0.167. All particle sizes are quoted as equivalent spherical volume diameters (ESVD). A further set of models were done for a three-dimensional cruciform shape consisting of three mutually perpendicular parallelepiped limbs intersecting each other at their center, where each parallelepiped has a relative dimension of 1x1x7, similar to that reported by Tauxe et al. (2002). Seventeen such models were made for ESVD particle sizes of 40 nm to 200 nm in 10 nm steps.

The Day plot parameters of M_{rs}, B_{c} and B_{cr} were obtained from simulated First Order Reversal Curves, described in Nagy et al. (2024) peak fields of 200 mT and maximum field steps of 4 mT. Hysteresis was performed by first saturating the magnetization in the direction of the applied field, and thereafter the initial guess at each field step was the local energy minimum magnetic domain structure solution of the previous field step. For each particle, we use an average of 29 different field directions from a Fibonacci distribution

(Hannay & Nye, 2004) over an octant of the sphere between azimuthal angles $\phi = 0$, $\pi/2$ and polar angle $\theta = 0$, $\pi/2$ symmetric to the particle elongation along $\langle 100 \rangle$. Back-field curves, again at increments of 4 mT, were generated for the 29 different field directions and averaged before extracting the M_{rs}, B_{c} and B_{cr} for each particle size and morphology.

3 Results

Almost all domain states modeled here with ESVD particle sizes between 40 nm to 200 nm are either SD or SV, but within these primary types of states, the magnetization can align along the easy or hard magnetocrystalline directions, or the short or long particle shape axes.

Example domain states are shown in Figure 2. We see that prolate particles (Figure 2 a,b,c) have their magnetization and vortex cores aligned along the easy shape (long) axis, but as particle size grows, the vortex core shape and orientation can distort e.g., Figure 2c. Particles whose size is close to the critical single domain particle size, d_{c}, will gradually change their domain state from SD to SV, becoming less uniform by exhibiting 'flowering' of the magnetization at the particle surface e.g., Figure 2e (Williams & Dunlop, 1990) where the domain state classification is not clear. Larger SD oblate particles form 'S' states within the oblate plane e.g., Figure 2h (Zhao et al., 2014). Occasionally 200 nm oblate particles formed MV states, e.g., Figure 2i. Each of these slight variations influences the particles' $M_{\mathrm{rs}}/M_{\mathrm{s}}$ and $B_{\mathrm{cr}}/B_{\mathrm{c}}$ values.

Each modelled mono-dispersion consists of 29 particles whose domain states are frequently of the same type, but variations may occur due to the different directions of the applied field. This is more common for particle sizes close to d_{c}, where some particles will nucleate SV states while others will remain in the SD state. For the largest particle sizes, almost all are in the SV state, but vortex core curvature can be present. In our models, some domain structures such as the 'S' state were found only in oblate particle morphologies. The MV domain state was only found in particles with AR=0.25, and only for 18 of the 29 particles in our mono-dispersion.

The predicted Day plot parameters for ellipsoidal magnetite are shown in Figure 3. These predominantly SD and SV particles often plot outside the $M_{\mathrm{rs}}/M_{\mathrm{s}}$ and $B_{\mathrm{cr}}/B_{\mathrm{c}}$ limits for SD and PSD particles, but nevertheless fall within a well-defined diagonal band across the (log-log) Day plot. Cruciform models are only included in the enlarged section in Figure 4.

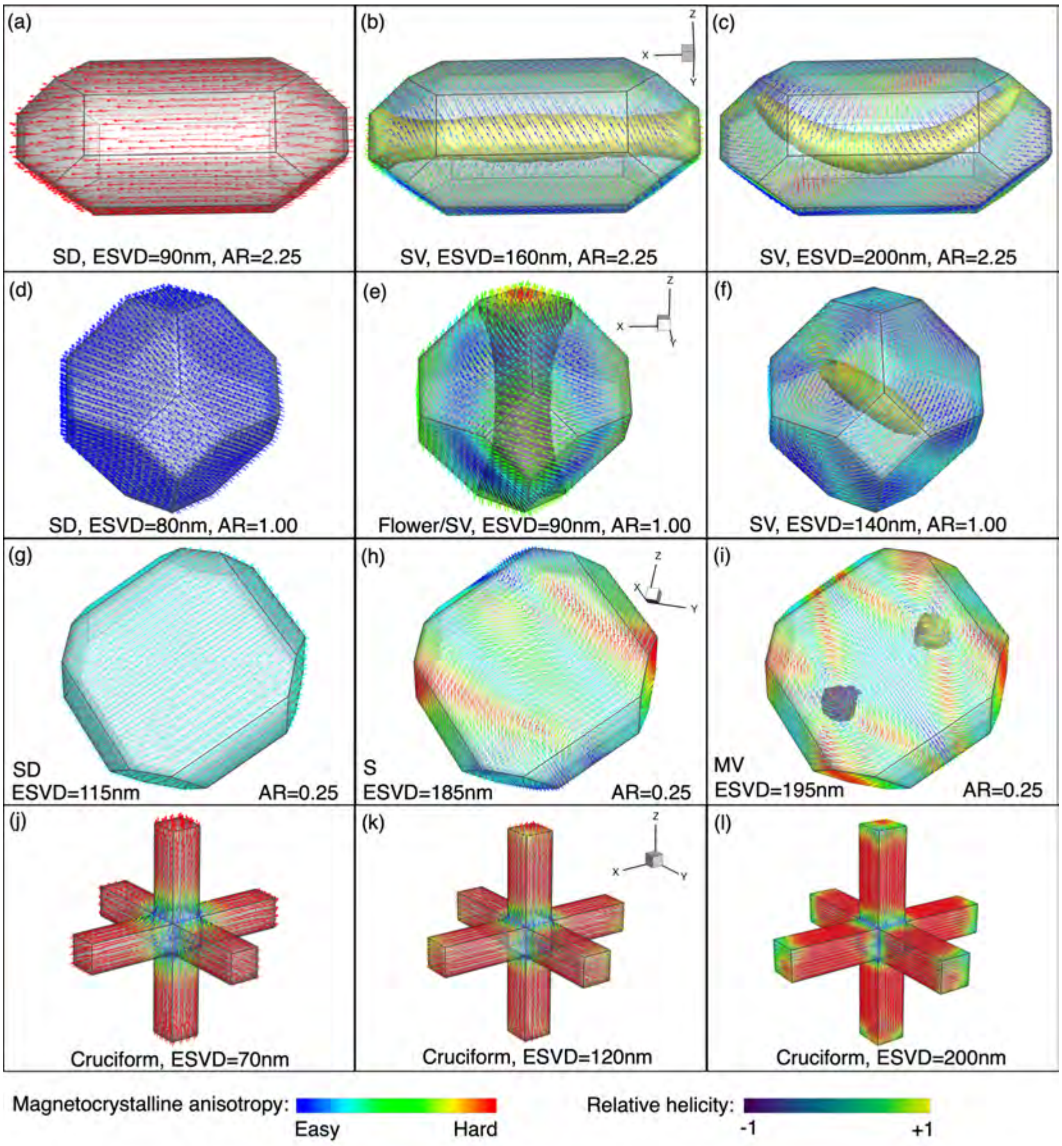

Figure 2. A selection of typical domain states that are nucleated as a function of particle size (ESVD) and shape (AR). The orientation of particles within each row is the same and indicated by the axes in the centre panel where x, y, z are along [100], [010] and [001] respectively. The magnetic structures are shown as surface vectors colored according to alignment with the cubic magnetocrystalline anisotropy. Where vortex structures are nucleated within the particle, its helicity isosurface is shown at ±95% of its maximum value. Each truncated-octahedral particle domain state is labelled as single-domain (SD), single-vortex (SV), S-state (S) or multi-vortex (MV). Domain states in cruciform particles are SD-like within each limb.

3.1 Behavior of SD particles on the Day plot

Regardless of particle morphology, only SD states should exist above $M_{\mathrm{rs}}/M_{\mathrm{s}} = 0.5$. In this study we take SD states to include different degrees of flowering and 'S-type' states;

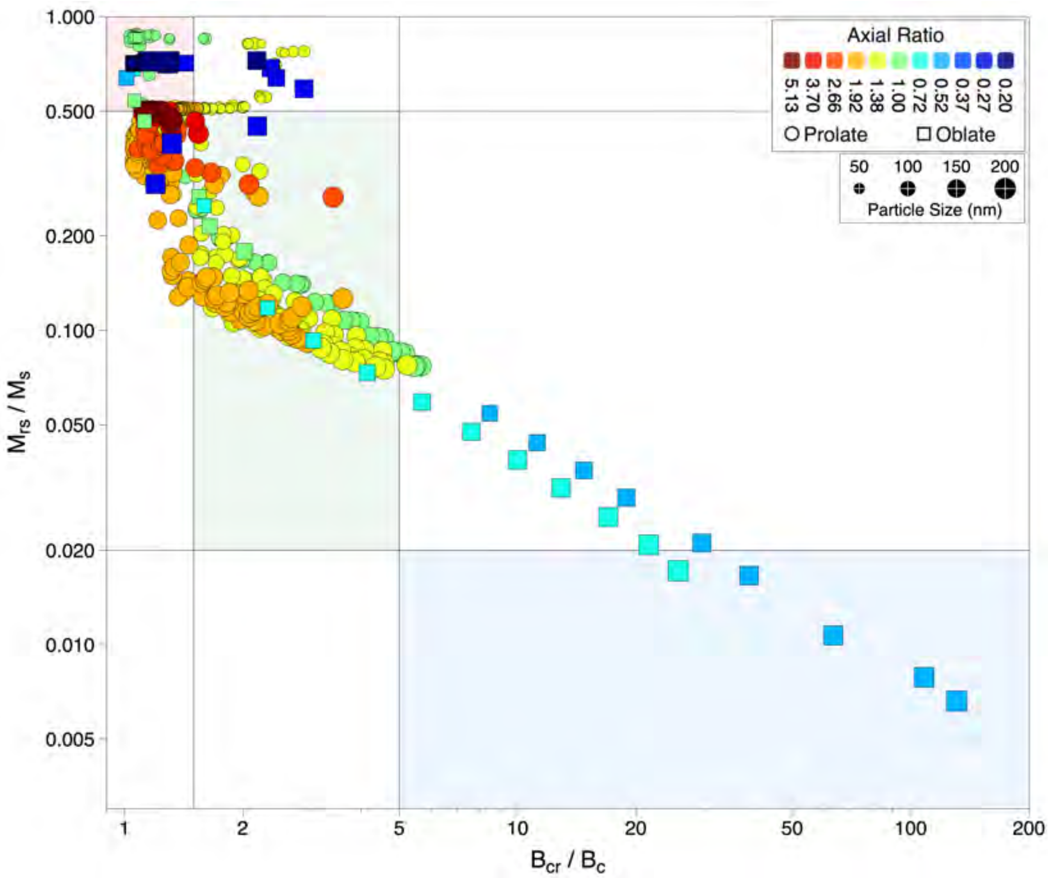

Figure 3. Plot of $M_{\rm rs}/M_{\rm s}$ versus $\mathrm{B}_{cr}/\mathrm{B}_c$ for simulated magnetite with increasing particle size and axial ratio. The oblate and prolate particles are represented by square and round symbols respectively, and colored according to their axial ratio. The symbol sizes are proportional to the particle sizes. The single domain, pseudo-single-domain, and multi-domain region proposed by (Day et al., 1977) are indicated by the lightly shaded red, green and blue regions respectively.

'S-type' states are treated as SD as they do not contain a vortex core (see Figure 2h), although in some cases these will report values of $M_{\rm rs}/M_{\rm s}$ lower than 0.5. In general, $M_{\rm rs}/M_{\rm s}$ values of random distributions of SD particles are controlled by their magnetic anisotropy, either crystalline or particle shape, or a combination of the two (e.g., Dunlop & Özdemir, 2010). For mono-dispersions of SD particles we expect our models to agree with analytic calculations for $M_{\rm rs}/M_{\rm s}$ that are easily determined using:

$$M_{\rm rs}/M_{\rm s} = \int_{\theta_{min}}^{\theta_{max}} \int_{\phi_{min}}^{\phi_{max}} \hat{\mathbf{m}} \cdot \hat{\mathbf{h}} \tag{1}$$

where ϕ and θ are the spherical coordinate azimuth and polar angle respectively. $M_{\rm rs}/M_{\rm s}$ will decrease with the number of dominant anisotropy axes as shown in (Table 1).

Table 1. $M_{\mathrm{rs}}/M_{\mathrm{s}}$ ratios for SD particles for various magnetic anisotropy symmetries determined using Eq. 1. The specified integration limits for the azimuthal angle (ϕ) and polar angle (θ) define the symmetry of the anisotropy about the given easy direction for each anisotropy type.

anisotropy type	$M_{\mathrm{rs}}/M_{\mathrm{s}}$	easy direction	θ limits	ϕ limits
Uniaxial	0.500	[1,0,0]	0, $\pi/2$	0, 2π
3 fold in basal plane	0.649	$\frac{1}{2}[1,\sqrt{3},0]$	0, $\pi/2$	0, $2\pi/3$
4 fold in basal plane	0.707	$\frac{1}{\sqrt{2}}[1,1,0]$	0, $\pi/2$	0, $\pi/2$
6 fold in basal plane	0.750	$\frac{1}{2}[\sqrt{3},1,0]$	0, $\pi/2$	0, $\pi/3$
Easy basal plane	0.785	$[\cos\phi, \sin\phi, 0]$	0, $\pi/2$	0, 2π
Cubic K>0	0.832	[1,0,0]	0, θ_{mid} †	0, 2π
Cubic K<0	0.866	$\frac{1}{\sqrt{3}}[1,1,1]$	0, $\pi/2$	0, 2π

† $\theta_{mid} = \tan^{-1}(\frac{1}{\cos\phi})$

Experimental observations of SD particles with $M_{\mathrm{rs}}/M_{\mathrm{s}} < 0.5$ will indicate the presence of significant magnetic particle interactions (Muxworthy et al., 2003), and/or a particle size distribution that exceeds the very narrow SD particle size range, or a particle size distribution that includes significant SP particles (Tauxe et al., 1996). For our modelled mono-dispersions, the enlarged section of the Day plot (Figure 4) shows three distinct groupings of $M_{\mathrm{rs}}/M_{\mathrm{s}}$ values that are distinctive to SD particles with a set anisotropy symmetry. The first is at $M_{\mathrm{rs}} = 0.87$, which reflects the cubic magnetocrystalline anisotropy expressed in near equidimensional particles (AR ≈ 1, colored green in Figure 4). The second group is at $M_{\mathrm{rs}}/M_{\mathrm{s}} \sim 0.71$ expected for highly oblate particles (AR $\lessapprox 0.5$, colored blue) with a 4-fold projection of the cubic magnetocrystalline anisotropy into the oblate plane (see Table 1). The third group is for highly prolate particles (AR $\gtrapprox 1.3$, colored orange to red), where the uniaxial shape anisotropy dominates, yielding $M_{\mathrm{rs}}/M_{\mathrm{s}} \sim 0.5$.

Similarly, analytical calculations of $B_{\mathrm{cr}}/B_{\mathrm{c}}$ for distributions of SD particles with coherent switching (Joffe & Heubregbr, 1974) predict that $B_{\mathrm{cr}}/B_{\mathrm{c}}$ is also influenced by magnetic anisotropy, but to a lesser degree. For a distribution of particles with the same anisotropy symmetry we expect the following $B_{\mathrm{cr}}/B_{\mathrm{c}}$ ratios: 1.08 (uniaxial), 1.15 (platelets) and 1.04/1.09 (positive/negative cubic)(Joffe & Heubregbr, 1974). For a distribution of SD particles with mixed anisotropies, Gaunt (1960) obtained $B_{\mathrm{cr}}/B_{\mathrm{c}} \lessapprox 2$. While our models broadly agree with these analytic predictions, in some cases, we can obtain $B_{\mathrm{cr}}/B_{\mathrm{c}}$ ratios approaching 3.0 even for particles of the same anisotropy form, but where neither shape nor magnetocrystalline anisotropies dominate, producing a more complex overall magnetic anisotropy. This occurs in particles with AR values ≈ 1.3 (yellow points) and ≈ 0.25 (medium blue points) for prolate and oblate particles respectively.

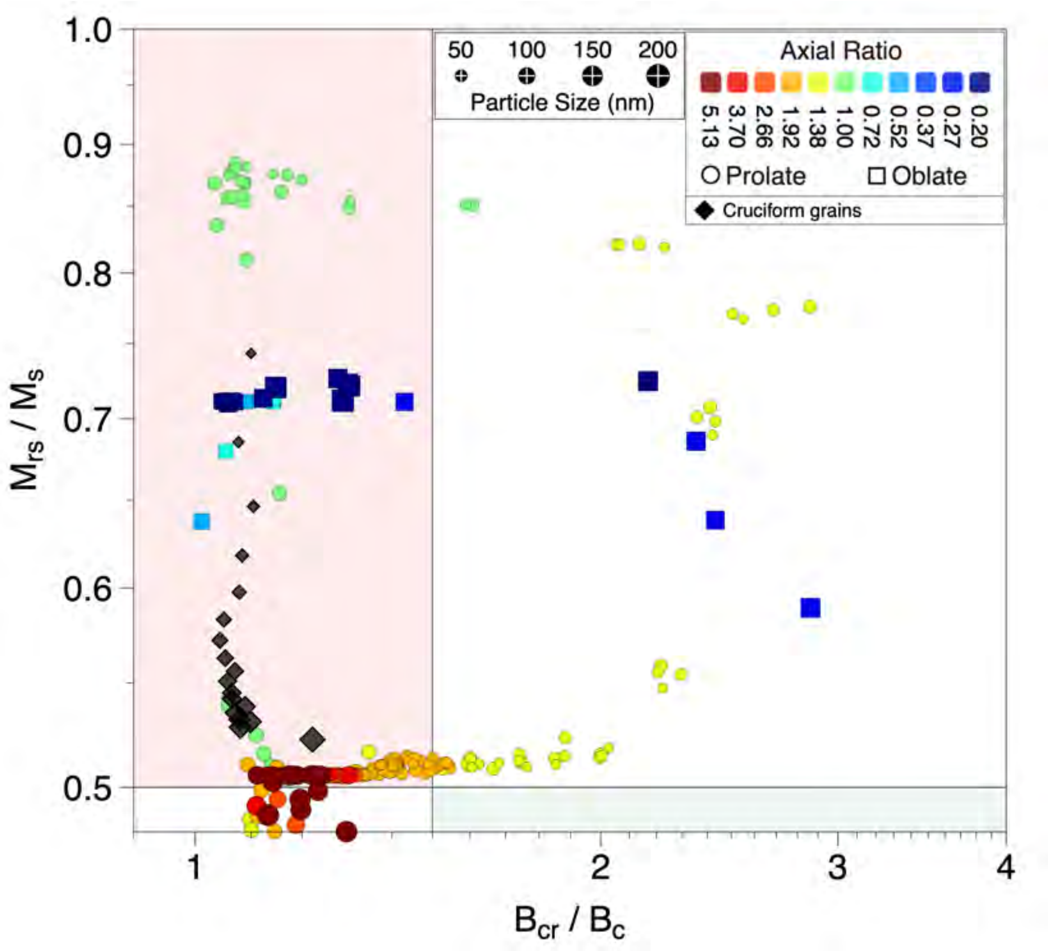

Figure 4. An enlarged section of Figure 3 showing the variation of the Day plot parameters for modelled mono-dispersions of SD particles. The symbols are colored according to the particle's AR, with circles and squares used for prolate and oblate particles respectively for additional clarity. The cruciform structures are shown as black diamonds. The symbol sizes are proportional to the particle sizes. The Day plot SD, and PSD regions are colored as Figure 3.

In addition to prolate and oblate particles, the modeled cruciform structures represent the more complex 'skeletal' particle structures observed in many basalts (Tauxe et al., 2002). In these morphologies, all of the particles up to the maximum modeled size of 200 nm are SD, with the magnetization in each limb aligned to the limb axis. As the particle size increases, the magnetization at the end of each limb becomes increasingly flowered (e.g., Figure 2j-l), which causes $M_{\rm rs}/M_{\rm s}$ to gradually decrease with increasing ESVD particle size from a maximum of 0.74 for the 40 nm particle to 0.52 at 200 nm. The cruciform structures have $B_{\rm cr}/B_{\rm c}$ values that remain relatively constant between 1.04 and 1.1. Hidden in the $B_{\rm cr}/B_{\rm c}$ ratio is the fact that the coercivity ($B_{\rm c}$) of the cruciform particles can be much larger than that expected for SD particles, which was the reason why (Tauxe et al., 2002) argued for plotting $M_{\rm rs}/M_{\rm s}$ against $B_{\rm c}$ and $B_{\rm cr}$ separately.

3.2 Behavior of SV particles on the Day plot

The Day plot parameters for modeled SV prolate particles fall within the PSD boundaries of $0.02 < M_{\rm rs}/M_{\rm s} < 0.5$ but slightly outside the $1.5 < B_{\rm cr}/B_{\rm c} < 4$ limits, as defined by (Day et al., 1977). Immediately below the $M_{\rm rs}/M_{\rm s} = 0.5$ boundary, domain states in any particular particle size are generally a combination of SD and SV, with SV states increasingly dominant as $M_{\rm rs}$ falls further. As the particle size of prolate-shaped particles increases the $M_{\rm rs}/M_{\rm s}$ decreases, reflecting smaller vortex cores that carry the remanence. Likewise, $B_{\rm cr}/B_{\rm c}$ also falls, reflecting increasing internal demagnetizing fields as well as the non-coherent domain state switching of the vortex core, referred to as structure coherent rotation (Nagy, Williams, Tauxe, Muxworthy, & Ferreira, 2019). For particles of a particular size, increasing elongation or contraction drives a change towards the SD state. SV oblate particles of moderate AR values of ~ 0.6 have Day-plot parameters that fall well into the MD region. Our study only considers particles with a maximum ESVD size of 200 nm, well below the expected transition to MV states at ~ 3 μm (Nagy, Williams, Tauxe, & Muxworthy, 2019), and that the trend line for SV particles seen in Figure 3 might continue into the MD region for all particle morphologies.

4 Discussion

The Day Plot attempts to characterize the domain state/particle size of an assemblage of magnetic particles in a sample using the ratio of four experimentally measured parameters, i.e., $M_{\rm rs}/M_{\rm s}$ and $B_{\rm cr}/B_{\rm c}$. While there have been many studies on the merits and shortfalls in using Day plots as indicators of domain state, until recently it has not been possible to account for the presence of pseudo-single-domain (PSD) states. Within the SV particle size range, the vortex structure will distort to accommodate irregular and asymmetric particle morphologies, and so we regard asymmetric SV domain states to be included within this broad category. Numerical micromagnetic models provide an insight into magnetic behavior in idealized stochiometric mineral structures by relaxing the constraint of uniform magnetization and coherent domain state switching that have limited much of our present understanding of magnetic recordings in paleomagnetic samples.

4.1 The Day plot's ability to discriminate particle size

Of the two ratios, the variation of $M_{\rm rs}/M_{\rm s}$ with particle size is the easiest to predict and understand. For a population of SD particles, in the absence of significant amounts of superparamagnetic particles, extensive ‘flowering’ or inter-particle magnetic interactions, $M_{\mathrm{rs}}/M_{\mathrm{s}}$ does not fall below 0.5. In contrast, our models predict that no SV states are possible with $M_{\mathrm{rs}}/M_{\mathrm{s}} > 0.5$ (Figure 5a), however, this ratio by itself is not a direct indicator of particle size due to non-uniqueness in $M_{\mathrm{rs}}/M_{\mathrm{s}}$. Since B_{c} and B_{cr} reflect both reversible and irreversible domain state changes as a function of the applied field, it is anticipated that non-coherent switching mechanisms that dominate in larger particle sizes will also affect the $B_{\mathrm{cr}}/B_{\mathrm{c}}$ ratio. Dunlop and Özdemir (2010) notes that non-coherent switching will result in lower critical fields and thus result in lower B_{cr} yielding lower $B_{\mathrm{cr}}/B_{\mathrm{c}}$ ratios. We might expect $B_{\mathrm{cr}}/B_{\mathrm{c}}$ to decrease for SD particles as they near the critical particle size where SD switching can occur via a transitory vortex state (Enkin & Williams, 1994). While this effect is imperceptible in most mono-dispersions of a single anisotropy, Figure 6 shows that a decrease in B_{cr} is noticeable for particles with AR=1.0 and AR=1.25 as the particle size grows towards the critical particle size of $\approx$ 80 nm and $\approx$ 90 nm respectively (Muxworthy & Williams, 2006; Butler & Banerjee, 1975; Moreno et al., 2022).

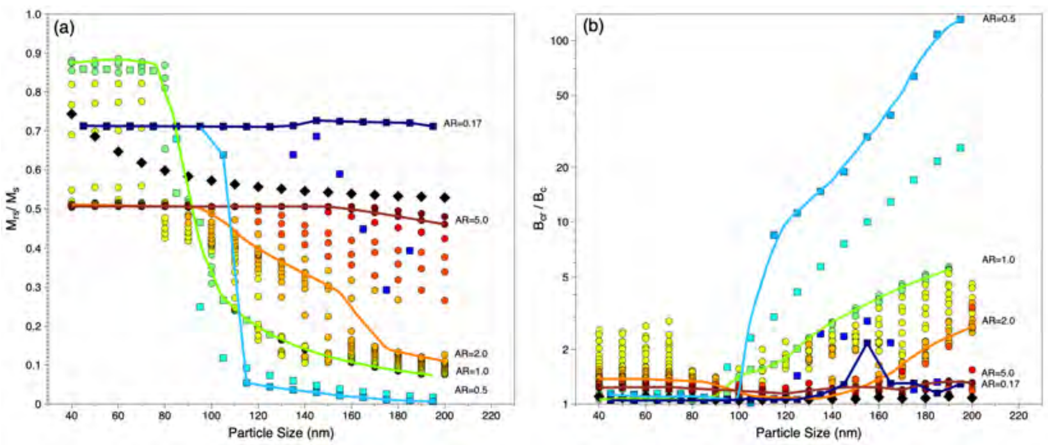

Figure 5. Plot of (a) $M_{\mathrm{rs}}/M_{\mathrm{s}}$ and (b) $B_{\mathrm{cr}}/B_{\mathrm{c}}$ versus particles size (ESVD) for randomly aligned mono-dispersions of truncated-octahedral magnetite of different axial ratios, as well as 3D cruciform geometries. The data is colored according to the particle’s AR. Guide lines for particles of selected equal ARs have been drawn for clarity.

4.2 The effect of particle shape

The trend line for SV domain states on the log-log Day plot (Figure 3) is remarkably linear within the 40 nm - 200 nm particle size range modelled. The lack of scatter in the data is in part due to the single truncated-octaheral particle shape in this study which has been elongated or compressed to form prolate or oblate morphologies. All prolate and oblate

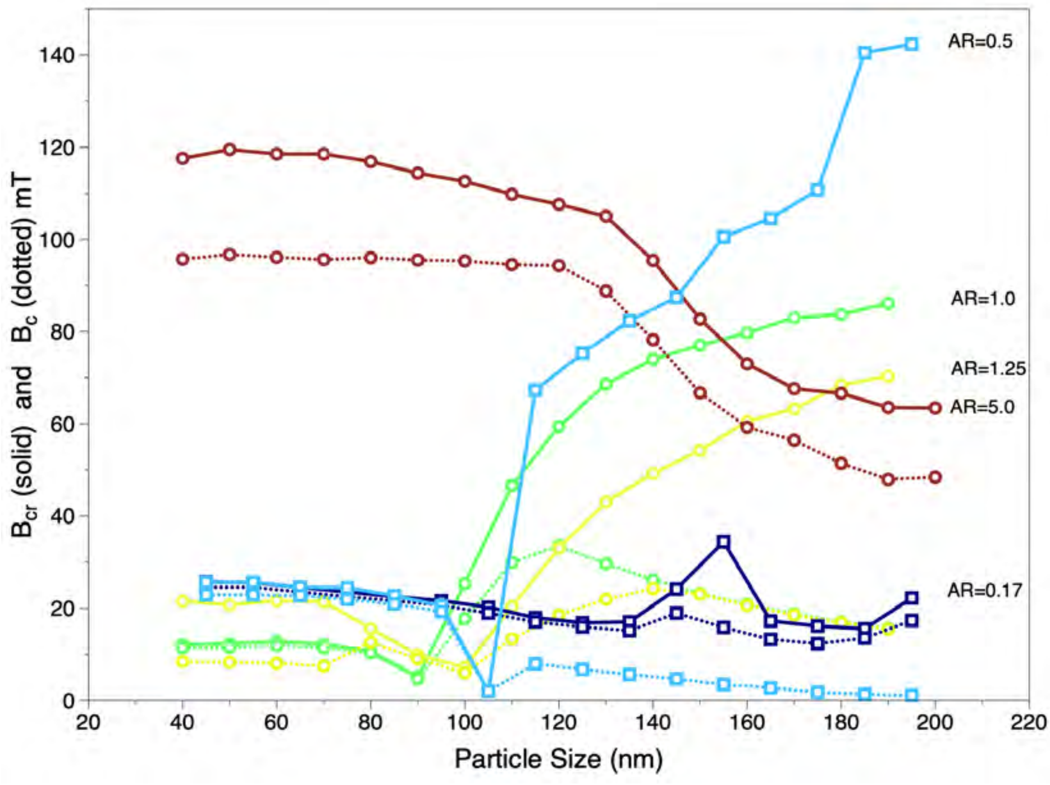

Figure 6. Plot of $B_{\rm cr}$ (solid lines) and $B_{\rm c}$ (dotted lines) versus particles size for randomly aligned mono-dispersions of truncated-octahedral magnetite of different selected axial ratios.

particles below 195 nm nucleate domain states that are either in the SD or SV state. In Figure 7 we compare our data against the simulated Day plot parameters in particles with irregular particle morphologies from Nikolaisen et al. (2020). Since almost all of the irregular particles are triaxial, the matching can only be approximate. Nevertheless, there is a good agreement between the Day plot trend from the irregular data and that from our idealized prolate and oblate particles.

It is worth noting that several irregular geometries (marked with hexagons in Figure 7) are stated to have MV domain states (see Figure 5 of (Nikolaisen et al., 2020)), and yet their Day plot parameters place them near the SD-SV boundary. As these contradict our results indicating that no multivortex state should yield $M_{\rm rs}/M_{\rm s}$ values greater than 0.5, we further investigate these specific morphologies from (Nikolaisen et al., 2020) by re-running their local energy minimum. For each of these published irregular geometries, we have calculated 100 models starting from different random initial states. Our results show that these irregular particle structures support a variety of domain states (see supplementary information Figure S1) , with particles as small as 163 nm sometimes being able to host MV domain states. A greater variety of domain states in these cases, also reflect a variety of final energies for each of these 100 solutions. In many of these geometries, the MV states are often one of the higher energy states and occur less frequently. In such particles, simulated hysteresis and backfield measurements will inevitably average over several domain states nucleated as a result of the varying direction of the applied field. Consequently, these are likely to be dominated by the lower energy domain, often SV, states and the saturated remanence states during hysteresis. Two particles highlighted in Figure 7, OPX39 and OPX22, both have MV structures as their lowest energy states, but even for these particles they yield $M_{\rm rs}/M_{\rm s}$ values well above that expected in MD states and are likely to hold stable magnetic remanences (Shah et al., 2018). The overall good agreement between the idealised particle morphologies and the irregular particles suggests that, as in the case of SD particles, much of the general behavior of SV/PSD particles can be determined from examining simple particle geometries.

4.3 Comparison to analytic models (mixing models)

So far we have considered Day plot parameters for mono-dispersions of particles of idealised morphologies, but experimental observations (except for samples created by etching of thin films (Krása et al., 2009; King et al., 1996)) will inevitably be representative of a variety of particle sizes and domain states. Dunlop (2002a) explored the Day plot phase space in terms of mixtures of SD and MD particles, and concluded that such mixtures can plot in the PSD region for a wide range of SD/MD mixtures; the mixing models are shown in Figure 8a. Dunlop (2002a) demonstrates that while the presence of SP particles can significantly increase $B_{\rm cr}/B_{\rm c}$, $M_{\rm rs}/M_{\rm s}$ never decreases below ≈ 0.09, even for samples containing $> 80\%$ SP fraction; such mixtures should be easily distinguished from samples dominated by MD particles. Mixtures of ideal SD and MD particles produce trend lines that fall within the expected PSD Day plot region, and demonstrate that samples containing such mixtures cannot be distinguished from samples dominated by PSD particles. The SD+MD mixture trend lines were formulated to explain Day plot behavior in the absence of any detailed understanding of the hysteresis in PSD particles. The calculations presented in this paper, together with the work of Nikolaisen et al. (2020), demonstrate that mono-dispersions of SV particles fall within the expected Day plot region for PSD particles without the need to consider mixtures of other domain states.

Within the range of particle sizes of our numerical solutions, we can construct more realistic size distributions by linearly averaging the hysteresis and remanence backfield curves with suitable weightings. In Figure 8b we show Day plot parameters for 24 lognormal distributions plotted together with the experimental observations on sized mono-dispersions. The Day plot parameters for the lognormal distributions can be generated from our Synth-FORC application at https://synth-forc.earthref.org (Nagy et al., n.d.) Each modelled distribution

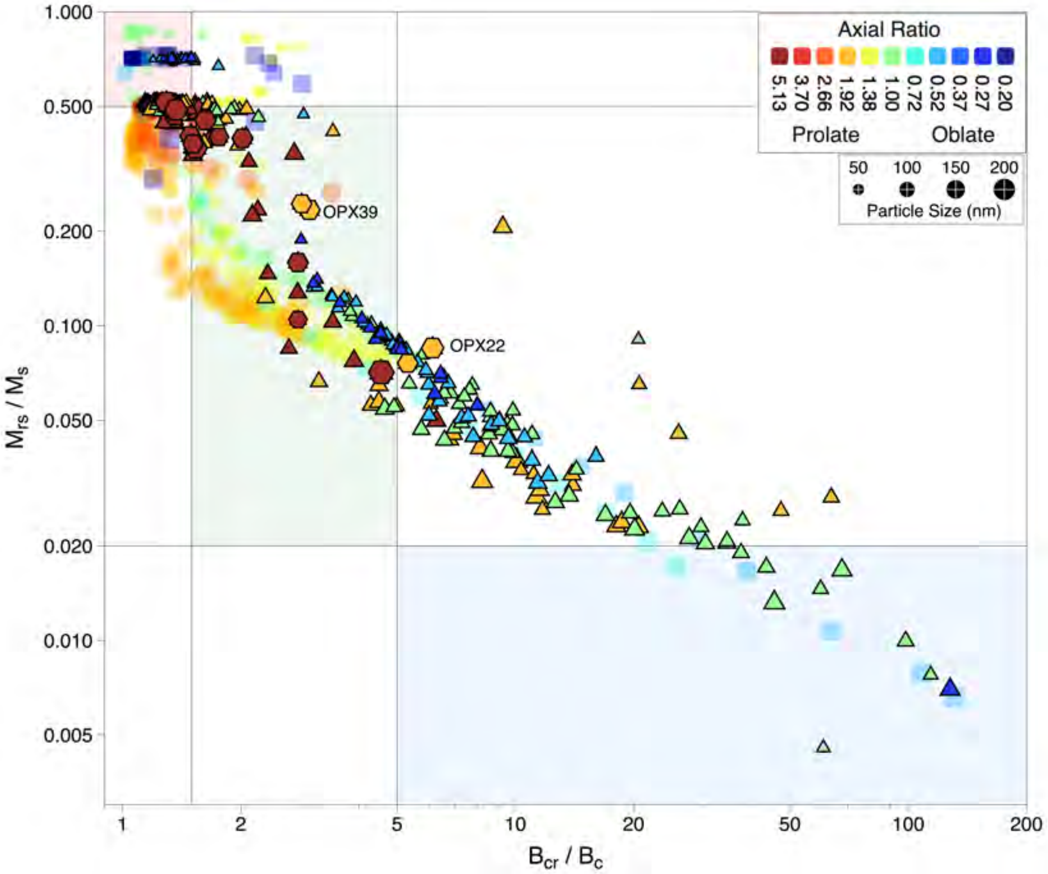

Figure 7. The Day Plot of irregular particle morphologies from (Nikolaisen et al., 2020). Colored triangles and hexagons are superimposed on the data of prolate and oblate truncated-octahedral particles from this study (made translucent for clarity). The data from (Nikolaisen et al., 2020) have been coloured according to their parameter ob-pro-sph=log((a -b)/(b-c)), where a,b,c are the particle long, intermediate and short axis lengths, and scaled to match the axial ratio range of this study. The triangle symbols indicate SD or SV domains states, while the hexagons indicate multi-vortex (MV) states. The symbol sizes are scaled with particles size in the same way for both data sets.

is characterised by the geometric mean $\bar{d}$ and $\bar{AR}$ of the particle size and axial ratio respectively. The lognormal distributions are similar to those produced in the laboratory, e.g., samples of Argyle and Dunlop (1990) and Ge et al. (2021). The 24 distributions consist of two groups of different widths (variance) of particle size and the axial ratio of σ^2(axial ratio) $= \sigma^2$(size) $= 0.3$ or 1.0, chosen to bound the experimentally observed distribution widths. We consider three different mean axial ratios, $\bar{AR}$, of 0.5 (blue symbols), 1.0 (green symbols) and 2.0, (orange symbols) with distributions of equal $\bar{AR}$ joined by a black line. We then have four different mean particle sizes $\bar{d}$, of 50, 100, 150 and 200 nm, where the size of the symbol used is proportional to $\bar{d}$. The effect of averaging the hysteresis data and back-field curves is to move their Day plot parameters to the centroid of the bounding Day plot region containing the particles in the distribution. These averages suggest that the narrow range of axial ratios (AR ≈ 0.5) for oblate particles responsible for the very high $B_{\mathrm{cr}}/B_{\mathrm{c}}$ ratio seen in Figure 3 is quickly reduced and so not noticeable even in experimental mono-dispersions.

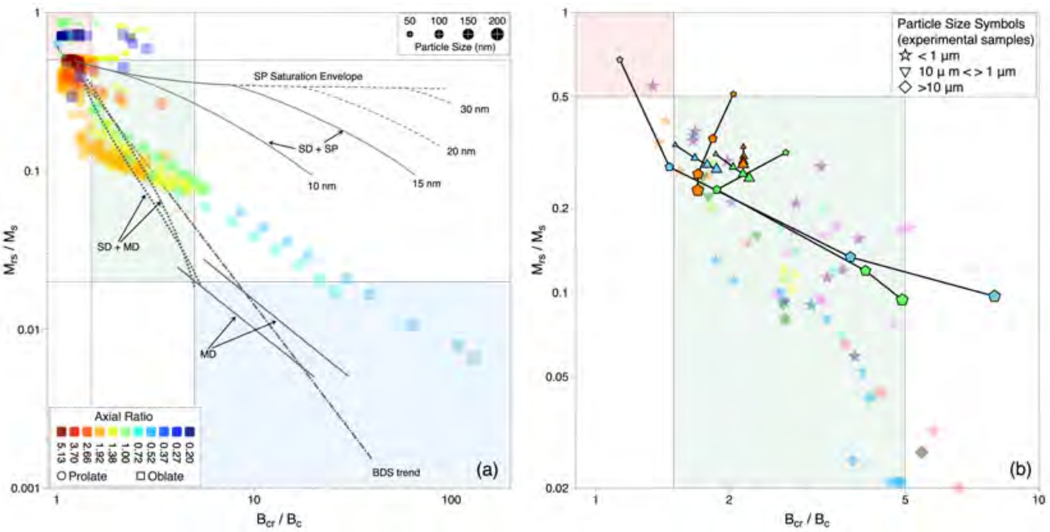

Figure 8. (a) The Day Plot of our numerical models (translucent dots and squares) compared to predictions from analytic models of domain state mixtures (grey lines), and (b) log-normal distributions of particle sizes and shapes from our numerical solutions (black lines and coloured diamonds). The lines for SD+MD, SD+SP and MD are from Dunlop (2002a), and the BDS (bulk domain stability) trend line is from Paterson et al. (2017). The modelled particle distributions shown in (b) are described in the text. The particle size and axial ratio legends apply to the model data for the mono-dispersions in (a) as well as to the geometric means of the modelled log-normal distributions in (b). The translucent colored stars, inverted triangles and diamonds are colored according to data attribution shown in Figure 9.

4.4 Comparison with experimental samples

In the original Day plot (Day et al., 1977) divisions of SD to PSD and PSD to MD were made relying on experimental observations in titanomagnetites together with theoretical limits of SD structures (Stoner & Wohlfarth, 1948; Butler & Banerjee, 1975). Since the Day plot was published, there have been attempts to validate the theoretical predictions by observations on well-characterized particle sized-dispersions of magnetites (Argyle &

Dunlop, 1990; Bailey & Dunlop, 1983; Day et al., 1977; Muxworthy & McClelland, 2000; Krása et al., 2011; Heider et al., 1996; Dankers & Sugiura, 1981; Dunlop, 1986; Özdemir & Banerjee, 1982; Muxworthy, 1998; Muxworthy et al., 2006); many of these are shown in Figure 9. Except for the elongated particles of Dunlop (1986), the experimental data are from near equidimensional particles, similar to the geometries used in our models. While there is generally good agreement, the experimental data do not display the high $B_{\mathrm{cr}}/B_{\mathrm{c}}$ values predicted for oblate particles of our study nor the highly irregular triaxial particles geometries of (Nikolaisen et al., 2020). This is likely due to averaging effects seen in broader particle size distributions.

For equidimensional particles, there is a noticeable difference in the gradient of the ratio of $(M_{\mathrm{rs}}/M_{\mathrm{s}})/(B_{\mathrm{cr}}/B_{\mathrm{c}})$ in the PSD particles size region, with this being larger for the experimental mono-dispersions than in the numerical models. However, the production of laboratory-manufactured samples that are true analogues of natural rocks is very difficult. In addition to the sized natural samples (labeled 'N' in the legend of Figure 9), there are three main types of laboratory samples: i) those that are sized by crushing larger particles; ii) those that are grown and remain un-crushed; (iii) and those that are produced by etching epitaxial films to produce specific particle sizes and inter-particle separations, noted by the letters 'C', 'G' and 'E' (Figure 9). Each method has its advantages and disadvantages, with only the etched samples guaranteed to be free from inter-particle magnetostatic interactions. These few samples appear to be in better agreement with the numerical models. Nevertheless, they are also likely to be significantly stressed due to the mismatch between the unit cell size of magnetite and that of the ruby substrate upon which they were grown (Krása et al., 2011; King et al., 1996). Powdered samples suffer from the effects of magnetostatic interactions, which is to decrease $M_{\mathrm{rs}}/M_{\mathrm{s}}$ (and to a lesser extent $B_{\mathrm{cr}}/B_{\mathrm{c}}$ (Muxworthy et al., 2003)). The latter will consequently bias the experimental data towards steeper gradients on the Day Plot. Within these limitations, there is still good agreement between the properties of laboratory-produced particles and our numerical simulations.

4.5 Alternatives to the Day Plot

The benefit of plotting M_{rs} normalized by M_{s}, and B_{cr} normalized by B_{c} is that for SD particles these ratios should be independent of mineralogy, except where that is expressed in their different magnetic anisotropies; the SD Day plot region should be distinct across different experimental samples. This is not necessarily true for distributions of MD particles, as clearly shown in the case of hematite described by Özdemir and Dunlop (2014). The low intrinsic magnetization of hematite results in weak internal demagnetizing fields, H_d, such that domain wall motion is determined almost entirely by the externally applied field. Thus,

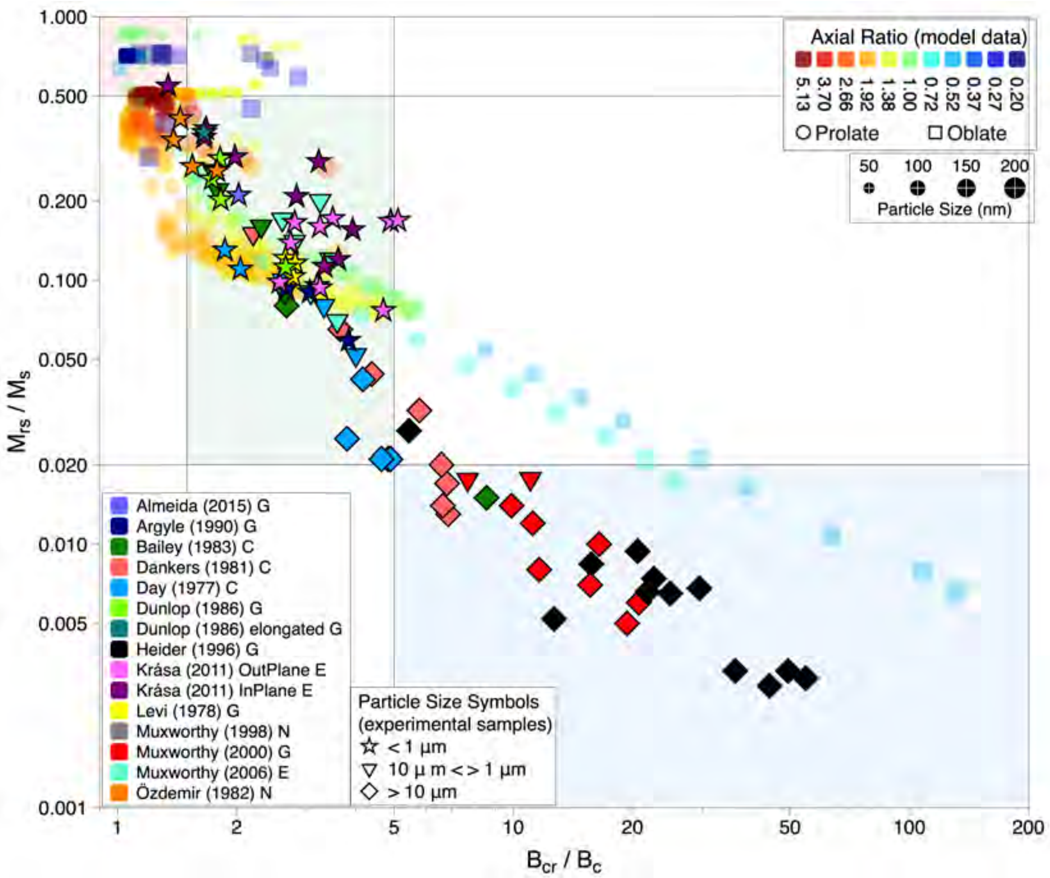

Figure 9. Plot of our modeled Day Plot parameters, (translucent) colored by their axial ratio, against those of sized experimental samples in black outlined symbols, colored to identify the original study from which the data has been obtained. The experimental samples are also categorized by their laboratory particle processing as, grown (G), crushed (C), etched thin films (E) or natural crystals (N). The thin film samples are further categorized by the hysteresis field applied in-plane or out-of-plane of the film. The experimental data uses different symbol shapes, shown in the legend, to identify the vortex to multidomain boundary, the lower limit of which is $\sim 1\mu m$ and the upper limit $\sim 10\mu m$.

values of $B_c \approx B_{cr}$ and near saturation values of M_{rs}/M_s often over 0.9 (Özdemir & Dunlop, 2014) are observed, far more than hematite's SD M_{rs}/M_s limit of 0.75.

Alternatives to the Day plot such as diagrams of M_{rs}/M_s against either B_c or against B_{cr}, first used by (Néel, 1955) and shown in Figure 10, have also been explored as a means of discrimination between magnetic domain states, e.g., (Tauxe et al., 2002). Generally, we expect coercivities to decrease with increasing particle size, as the domain switching mechanism changes from coherent rotation to non-coherent mechanisms, specifically vortex core rotation, and vortex core nucleation, translation and denucleation (Enkin & Williams, 1994). All non-coherent changes of domain states are indications that significant internal demagnetizing fields exist within a particle, but the absolute values will vary with mineralogy. With a single dominant mineralogy, the coercivities can sometimes also indicate particle morphology. For example, equidimensional magnetite particles have magnetocrystalline anisotropy-controlled coercivities no greater than ~ 37 mT (Williams & Dunlop, 1995) and values larger than this will indicate the presence of particles dominated by shape or configurational anisotropy. This is seen in Figure 10 in the case of prolate particles of similar $M_{\mathrm{rs}}/M_{\mathrm{s}}$ whose B_{c} and B_{cr} increases with AR (Tauxe et al., 2002). However this is not true in general, and neither oblate nor the more complex cruciform-shaped particles (or the traxial particles reported by Nikolaisen et al. (2020)) exhibit such a clear variation with AR.

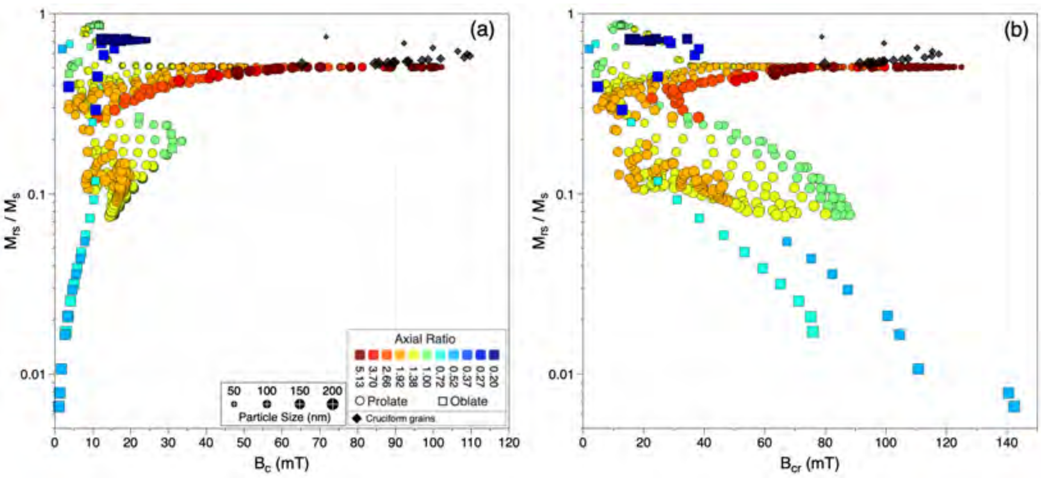

Figure 10. Plots of (a) $M_{\mathrm{rs}}/M_{\mathrm{s}}$ against B_{c}, often referred to a Néel plot of against, and (b)$M_{\mathrm{rs}}/M_{\mathrm{s}}$ and B$_{cr}$. The legend for the axial ratio and particle size apply to both plots.

Plotting $M_{\mathrm{rs}}/M_{\mathrm{s}}$ against B_{cr} (Figure 10b) does not yield a monotonic decrease in the abscissa we see in the Day plot. However, both M_{rs} and B_{cr} measure the remanence domain states that are important to paleomagnetic studies, rather than the induced domain states of in-field measurements. B_{cr} observations thus avoid the contamination of superparamagnetic (SP) and weakly stable (MD) states that lower both the value of $M_{\mathrm{rs}}/M_{\mathrm{s}}$ and $B_{\mathrm{cr}}/B_{\mathrm{c}}$ (Dunlop, 2002a). This reduces the potential to place paleomagnetic samples containing SP mixtures with stable SD and SV particles into the MD region of the Day plot, which might falsely indicate the sample to be a poor paleomagnetic recorder. We might also expect B_{cr} to be an indicator of changing domain state because B_{cr} increases with the internal demagnetizing field, which acts to restore the domain state on removal of the external field. Increasing internal demagnetizing fields are also precursors to domain state changes, which form to minimize the internal field. We therefore expect to see a decrease in B_{cr} at the critical SD particle size d_{c} on the transition to SV states, and also at the critical vortex domain size d_{v} on the transition to MD states.

Near the SD-PSD boundary our models show there is a slight decrease in B_{cr} due to the nucleation of the vortex state, (Figure 5), but this is a subtle effect and is likely not resolvable in anything other than mono-dispersions. We might expect a larger change in B_{cr} near the transition to MD states at d_{c}. At present we are not able to model such large particles but the experimental observations on sized particle distributions (Figure 11 does show a marked decrease in B_{cr} at $\sim$ 1 to 10 μm, at the predicted size for d_{c} in magnetite (Nagy, Williams, Tauxe, & Muxworthy, 2019).

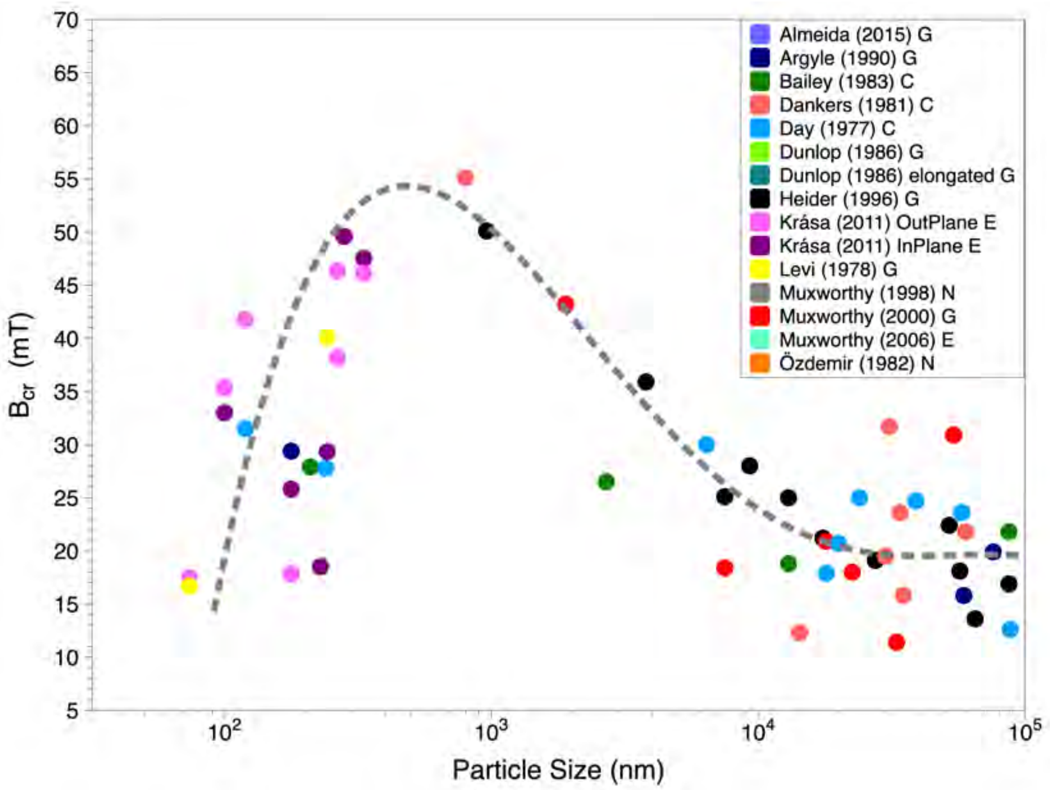

Figure 11. The variation of B_{cr} with particle size, from experimental observations on sized particle distributions. The symbols are colored according to data attribution as shown in the legend (as in Figure 9). The dashed grey line is drawn as a guide to the eye.

Thus, in the Day plot alternative of $M_{\mathrm{rs}}/M_{\mathrm{s}}$ against B_{rc}, the upper left of the plot should contain SD particles. $M_{\mathrm{rs}}/M_{\mathrm{s}}$ will decrease monotonically with particle size, but B_{cr} should rise and fall at each major transition in domain state. This is easily apparent experimentally in sized particle samples but likely difficult to distinguish in natural samples. Critically, absolute values of B_{cr} will depend on mineralogy, and so interpretation would depend on samples with a single dominant mineralogy, and availability of reference values for B_{cr} in SD, PSD and MD particles.

For example, hematite's easy basal plane anisotropy and weak magnetization results in MD particles with high values of $M_{\mathrm{rs}}/M_{\mathrm{s}}$ and low values of $B_{\mathrm{cr}}/B_{\mathrm{c}}$, and so they lie well into SD Day plot region (for a single dominant mineral, MD hematite is best identified by $M_{\mathrm{rs}} \sim 0.75$) Özdemir and Dunlop (2014). In this case, the Néel plot would yield high coercivities that might be diagnostic of a mineral such as hematite. Alternatively, since we expect B_{cr} to increase the value of the internal demagnetizing field H_{d}, we might expect B_{cr} to peak before a domain state change and so plotting $M_{\mathrm{rs}}/M_{\mathrm{s}}$ against B_{cr} would not only produce high values of B_{cr} that provides a guide to mineralogy, but its value should peak before a domain state change. Figure 11 suggests a peak in B_{cr} near 1 μm for magnetite, in broad agreement with the theoretically predicted value of $\sim$3 μm (Nagy, Williams, Tauxe, & Muxworthy, 2019), and the experimentally determined value of $\sim$0.8 μm (Dunlop & Özdemir, 2010) p153. However, the variation in B_{cr} with particle size is likely too weak to be used in any predictive test on paleomagnetic samples.

5 Conclusions

Characterization of the magnetic properties of a natural sample using a single data point can only ever be expected to provide a bulk estimate of its domain state, particle size or paleomagnetic stability. Each mono-dispersion that we model may contain a variety of domain states if more than one state is supported in particles of that size and shape. Usually, mono-dispersions will be dominated by one domain state type (SV or SD) except for particles near the critical SD particle size d_{c}. In our idealised shape and stoichiometric particles of magnetite (ranging from 40 nm - 200 nm), we observe a Day plot trend very similar to those predicted in irregular particle shapes (Nikolaisen et al., 2020). This suggests that despite the simple geometries we impose, they can make broad predictions of the hysteresis characteristics of particles in natural samples. Our predictions of Day plot parameters agree well with experimental observations on laboratory-manufactured samples, particularly when averaged over log-normal distributions typical of laboratory-made samples.

For SD particles, our results show that while we get the expected $M_{\mathrm{rs}}/M_{\mathrm{s}}$ values above 0.5, we can have $B_{\mathrm{cr}}/B_{\mathrm{c}}$ values as large as 3 for particles that have anisotropies dominated by neither shape nor magnetocrystalline (see Figure 4; these plot well outside the traditional $B_{\mathrm{cr}}/B_{\mathrm{c}}$ SD limit of 1.5 (Day et al., 1977). Mono-dispersions of SV domain states have $M_{\mathrm{rs}}/M_{\mathrm{s}}$ values below 0.5 and decrease with increasing particle size. For a narrow range of oblate morphologies that exhibit both shape and magnetocrystalline anisotropy (AR ≈ 0.2), we obtain $M_{\rm rs}/M_{\rm s}$ much smaller than the lower PSD limit of 0.02, and $B_{\rm cr}/B_{\rm c}$ far larger than 4 (Day et al., 1977) or 5 (Dunlop, 2002a) and so are more indicative of MD domain states. In our models of log-normal distributions of SD and SV domain states, the contribution of the relatively narrow band of SV particles with large $B_{\rm cr}/B_{\rm c}$ values is not noticeable. For natural samples, however, Nikolaisen et al. (2020) have reported a larger abundance of SV particles with large $B_{\rm cr}/B_{\rm c}$ values. We cannot therefore exclude the possibility that SV domain states will plot within the MD region of Day plot.

In bulk samples, there is a likelihood of a range of particle sizes and shapes, as well as a mixture of mineralogies. Often we are interested to know whether this mixture of mineral particles is capable of holding a reliable paleomagnetic signal. The theoretical confirmation that SV and MV are at least as magnetically stable as SD states (Nagy et al., 2017; Nagy, Williams, Tauxe, Muxworthy, & Ferreira, 2019; Shah et al., 2018) suggests that the most important discrimination should be between PSD and MD particles rather than SD and PSD. If that is accepted, then samples whose hysteresis parameters fall within the broad region of the SD and PSD Day plot region are likely to contain a significant proportion of paleomagnetically stable domain states.

While this assessment generally agrees with experimental and theoretical observations for magnetite, other minerals with distinct magnetic properties (such as the type and constant values of anisotropy) might produce $M_{\rm rs}/M_{\rm s}$ and $B_{\rm cr}/B_{\rm c}$ ratios that would falsely plot the particles in the stable SD/PSD regions of the Day plot (such as MD hematite). To better support the Day plot interpretation, a more in-depth characterization of the mineral morphology is suggested, which can be achieved by, e.g., thermal analysis of samples to identify blocking temperatures, and thermal demagnetization of IRM to examine the behavior of remanence-bearing particles.

The Day Plot (and Néel plots) remain a useful parameterization of hysteresis observations that can aid the identification of domain state stability. $M_{\rm rs}/M_{\rm s}$ itself is a strong discriminator of whether a sample's remanence is dominated by stable or unstable domain states. Using the parameter $B_{\rm cr}/B_{\rm c}$ provides a degree of normalization across different mineralogies, but this is not guaranteed as the case of hematite exemplifies. Absolute values of $B_{\rm c}$ and $B_{\rm cr}$ can identify Day plot 'outliers' but no one diagnostic test should be used in isolation.

6 Open Research

All results reported here were generated using the open source micromagnetic modeling code of Conbhuí et al. (2018). A complete guide to installation and use of MERRILL is described here: `https://rockmag.org`. The input scripts for generating the truncated-octahedral geometries and finite element meshes are provided in the supplementary information and the source code for MERRILL can be downloaded from `https://bitbucket.org/wynwilliams/merrill/` and is provided under a CC-BY-SA 4.0 International license.

Acknowledgments

W.W., R.M., A.R.M. and A.A.C. acknowledge support from UKRI NERC grants NE/S001018/1 and NE/V001388/1. G.A.P. NERC Independent Research Fellowship NE/P017266/1 and grant NE/W006707/1 L.T. acknowledges support from NSFGEO-NERC grant EAR2245628. L.N. acknowledges funding from Natural Environmental Research Council (NERC) Independent Research Fellowship (NE/V014722/1).

References

Almeida, T. P., Kasama, T., Muxworthy, A. R., Williams, W., Nagy, L., Hansen, T. W., ... Dunin-Borkowski, R. E. (2014). Visualized effect of oxidation on magnetic recording fidelity in pseudo-single-domain magnetite particles. *Nature Communications*, *5*, 5154. doi: 10.1038/ncomms6154

Argyle, K. S., & Dunlop, D. J. (1990). Low-temperature and high-temperature hysteresis of small multidomain magnetites (215-540 nm). *Journal of Geophysical Research-Solid Earth and Planets*, *95*(B5), 7069 - 7083. doi: 10.1029/jb095ib05p07069

Bailey, M. E., & Dunlop, D. J. (1983). Alternating field characteristics of pseudo-single domain (2-14 µm) and multidomain magnetite. *Earth and Planetary Science Letters*, *63*, 335–352.

Brown, W. (1963). Thermal fluctuations of a single-domain particle. *Physical Review*, *130*(5), 1677-1686.

Butler, R. F., & Banerjee, S. K. (1975). Theoretical single-domain grain size range in magnetite and titanomagnetite. *Journal of Geophysical Research: Solid Earth (1978–2012)*, *80*(29), 4049 – 4058. doi: 10.1029/jb080i029p04049

Conbhuí, P. O., Williams, W., Fabian, K., Ridley, P., Nagy, L., & Muxworthy, A. R. (2018). Merrill: Micromagnetic earth related robust interpreted language laboratory. *Geochemistry Geophysics Geosystems*, *19*(4), 1080 – 1106. doi: 10.1002/2017gc007279

Coreform LLC. (2017). *Coreform Cubit, v16.4 (64-Bit).* Retrieved from `https://coreform.com`

Dankers, P., & Sugiura, N. (1981). The effects of annealing and concentration on the hysteresis properties of magnetite around the psd-md transition. *Earth and Planetary Science Letters*, *56*, 422-428. doi: 10.1016/0012-821x(81)90145-x

Day, R., Fuller, M., & Schmidt, V. A. (1977). Hysteresis properties of titanomagnetites: Grain-size and compositional dependence. *Physics of the Earth and Planetary Interiors*, *13*(4), 260-267. doi: 10.1016/0031-9201(77)90108-x

Dunlop, D. J. (1986). Hysteresis properties of magnetite and their dependence on particle size: A test of pseudo-single-domain remanence models. *Journal of Geophysical Research: Solid Earth (1978–2012)*, *91*(B9), 9569 – 9584. doi: 10.1029/jb091ib09p09569

Dunlop, D. J. (2002a). Theory and application of the day plot (mrs/ msversus hcr/ hc) 1. theoretical curves and tests using titanomagnetite data. *Journal of Geophysical Research*, *107*(B3), 2056. doi: 10.1029/2001jb000486

Dunlop, D. J. (2002b). Theory and application of the day plot (mrs/ msversus hcr/ hc) 2. application to data for rocks, sediments, and soils. *Journal of Geophysical Research-Solid Earth and Planets*, *107*(B3), 333 – 15. doi: 10.1029/2001jb000487

Dunlop, D. J., & Özdemir, O. (2010). *Rock magnetism.* doi: 10.1017/cbo9780511612794

Enkin, R. J., & Williams, W. (1994). 3-dimensional micromagnetic analysis of stability in fine magnetic grains. *Journal of Geophysical Research-Solid Earth*, *99*(B1), 611-618. doi: Doi10.1029/93jb02637

Fletcher, E. J., & O'Reilly, W. (1974). Contribution of fe2+ ions to the magnetocrystalline anisotropy constant k1 of fe3–xtixo4 (0 ¡ x ¡ 0.1). *Journal of Physics C: Solid State Physics*, *7*, 171–178.

Gaunt, P. (1960). A magnetic study of precipitation in a gold-cobalt alloy. *Philosophical Magazine*, *5*(59), 1127-1145. doi: 10.1080/14786436008238321

Ge, K., Williams, W., Nagy, L., & Tauxe, L. (2021). Models of maghematization: Observational evidence in support of a magnetic unstable zone. *Geochemistry, Geophysics, Geosystems*, *22*(3). doi: 10.1029/2020gc009504

Hannay, J. H., & Nye, J. F. (2004). Fibonacci numerical integration on a sphere. *Journal of Physics A: Mathematical and General*, *37*(48), 11591. doi: 10.1088/0305-4470/37/48/005

Harrison, R. J., Dunin-Borkowski, R. E., & Putnis, A. (2002). Direct imaging of nanoscale magnetic interactions in minerals. *Proc Natl Acad Sci U S A*, *99*(26), 16556-61. doi: 10.1073/pnas.262514499

Heider, F., & Williams, W. (1988). Note on temperature-dependence of exchange constant in magnetite. *Geophysical Research Letters*, *15*(2), 184-187. doi: DOI10.1029/GL015i002p00184

Heider, F., Zitzelsberger, A., & Fabian, F. (1996). Magnetic susceptibility and remanent coercive force in grown magnetite crystals from 0.1 µm to 6 mm. *Physics of the Earth and Planetary Interiors*, *93*, 239-256.

Joffe, I., & Heubregbr, R. (1974). Hysteresis properties of distributions of cubic single-domain ferromagnetic particles. *Philosophical Magazine*, *29*(5), 1051–1059. doi: 10.1080/14786437408226590

King, J. G., & Williams, W. (2000). Low-temperature magnetic properties of magnetite. *Journal of Geophysical Research-Solid Earth*, *105*(B7), 16427-16436. doi: Doi10.1029/2000jb900006

King, J. G., Williams, W., Wilkinson, C. D. W., McVitie, S., & Chapman, J. N. (1996). Magnetic properties of magnetite arrays produced by the method of electron beam lithography. *Geophysical Research Letters*, *23*(20), 2847-2850. doi: Doi10.1029/96gl01371

Krása, D., Muxworthy, A. R., & Williams, W. (2011). Room- and low-temperature magnetic properties of 2-d magnetite particle arrays. *Geophysical Journal International*, *185*(1), 167-180. doi: 10.1111/j.1365-246X.2011.04956.x

Krása, D., Wilkinson, C. D. W., Gadegaard, N., Kong, X., Zhou, H., Roberts, A. P., ... Williams, W. (2009). Nanofabrication of two-dimensional arrays of magnetite particles for fundamental rock magnetic studies. *Journal of Geophysical Research*, *114*(B2). doi: 10.1029/2008jb006017

Lascu, I., Einsle, J. F., Ball, M. R., & Harrison, R. J. (2018). The vortex state in geologic materials: A micromagnetic perspective. *Journal of Geophysical Research: Solid Earth*, *123*(9), 7285–7304. doi: 10.1029/2018jb015909

Moreno, R., Carvalho-Santos, V., Altbir, D., & Chubykalo-Fesenko, O. (2022). Detailed examination of domain wall types, their widths and critical diameters in cylindrical magnetic nanowires. *Journal of Magnetism and Magnetic Materials*, *542*, 168495. doi: https://doi.org/10.1016/j.jmmm.2021.168495

Muxworthy, A. R. (1998). *Stability of magnetic remanence in multidomain magnetite* (Unpublished doctoral dissertation).

Muxworthy, A. R., King, J. G., & Odling, N. (2006). Magnetic hysteresis properties of interacting and noninteracting micron-sized magnetite produced by electron beam lithography. *Geochemistry, Geophysics, Geosystems*, *7*(7). doi: 10.1029/2006gc001309

Muxworthy, A. R., & McClelland, E. (2000). The causes of low-temperature demagnetization of remanence in multidomain magnetite. *Geophysical Journal International*, *140*, 115-131.

Muxworthy, A. R., & Williams, W. (2006). Critical single-domain/multidomain grain sizes in noninteracting and interacting elongated magnetite particles: Implications for magnetosomes. *Journal of Geophysical Research: Solid Earth (1978–2012)*, *111*(B12), B12S12-n/a. doi: 10.1029/2006JB004588

Muxworthy, A. R., Williams, W., & Virdee, D. (2003). Effect of magnetostatic interactions on the hysteresis parameters of single-domain and pseudo-single-domain grains. *Journal of Geophysical Research*, *108*(B11). doi: 10.1029/2003jb002588

Nagy, L., Moreno, R., Muxworthy, A. R., Williams, W., Paterson, G. A., Tauxe, L., & Valdez-Grijalva, M. (2024). Micromagnetic determination of the forc response of paleomagnetically significant magnetite assemblages. *ESS Open Archive*. doi: 10.22541/essoar.170533987.78411398/v1

Nagy, L., Moreno, R., Williams, W., Paterson, G., Tauxe, L., & Muxworthy, A. R. (n.d.). *Synth-forc* [webpage]. Retrieved from `https://synth-forc.earthref.org/`

Nagy, L., Williams, W., Muxworthy, A. R., Fabian, K., Almeida, T. P., Conbhui, P. O., & Shcherbakov, V. P. (2017). Stability of equidimensional pseudo-single-domain magnetite over billion-year timescales. *Proc Natl Acad Sci U S A*, *114*(39), 10356-10360. doi: 10.1073/pnas.1708344114

Nagy, L., Williams, W., Tauxe, L., & Muxworthy, A. R. (2019). From nano to micro: Evolution of magnetic domain structures in multidomain magnetite. *Geochemistry Geophysics Geosystems*, *20*(6), 2907 – 2918. doi: 10.1029/2019gc008319

Nagy, L., Williams, W., Tauxe, L., Muxworthy, A. R., & Ferreira, I. (2019). Thermomagnetic recording fidelity of nanometer-sized iron and implications for planetary magnetism. *Proceedings Of The National Academy Of Sciences Of The United States Of America*, *116*(6), 1984 – 1991. doi: 10.1073/pnas.1810797116

Néel, L. (1949). Théorie du traînage magnétique des ferromagnétiques en grains fins avec applications aux terres cuites. *Annales de Géophysique*, *5*, 99–136.

Néel, L. (1955). Some theoretical aspects of rock-magnetism. *Adv. Phys*, *4*, 191-243. doi: 10.1080/00018735500101204

Nikolaisen, E. S., Harrison, R. J., Fabian, K., & McEnroe, S. A. (2020). Hysteresis of natural magnetite ensembles: Micromagnetics of silicate-hosted magnetite inclusions based on focused-ion-beam nanotomography. *Geochemistry, Geophysics, Geosystems*, *21*(11). doi: 10.1029/2020gc009389

Özdemir, O., & Banerjee, S. K. (1982). A preliminary magnetic study of soil samples from west-central minnesota. *Earth and Planetary Science Letters*, *59*(2), 393-403. doi: 10.1016/0012-821x(82)90141-8

Özdemir, O., & Dunlop, D. J. (2014). Hysteresis and coercivity of hematite. *Journal of Geophysical Research: Solid Earth*, *119*(4), 2582-2594. doi: 10.1002/2013jb010739

Paterson, G. A., Muxworthy, A. R., Yamamoto, Y., & Pan, Y. (2017). Bulk magnetic domain stability controls paleointensity fidelity. *Proc Natl Acad Sci U S A*, *114*(50), 13120-13125. doi: 10.1073/pnas.1714047114

Pauthenet, R., & Bochirol, L. (1951). Aimantation spontanee des ferrites. *Journal De Physique et le Radium*, *12*(3), 249-251. doi: DOI10.1051/jphysrad:01951001203024900

Rave, W., Fabian, K., & Hubert, A. (1998). Magnetic states of small cubic particles with uniaxial anisotropy. *Journal of Magnetism and Magnetic Materials*, *190*(3), 332-348. doi: Doi10.1016/S0304-8853(98)00328-X

Roberts, A. P., Almeida, T. P., Church, N. S., Harrison, R. J., Heslop, D., Li, Y., … Zhao, X. (2017). Resolving the origin of pseudo-single domain magnetic behavior. *Journal of Geophysical Research: Solid Earth*, *122*(12), 9534-9558. doi: 10.1002/2017jb014860

Roberts, A. P., Hu, P., Harrison, R. J., Heslop, D., Muxworthy, A. R., Oda, H., … Zhao, X. (2019). Domain state diagnosis in rock magnetism: Evaluation of potential alternatives to the day diagram. *Journal of Geophysical Research: Solid Earth*, *124*(6), 5286–5314. doi: 10.1029/2018jb017049

Roberts, A. P., Pike, C. R., & Verosub, K. L. (2000). First-order reversal curve diagrams: A new tool for characterizing the magnetic properties of natural samples. *Journal of Geophysical Research: Solid Earth*, *105*(B12), 28461–28475. doi: 10.1029/2000jb900326

Roberts, A. P., Tauxe, L., Heslop, D., Zhao, X., & Jiang, Z. (2018). A critical appraisal of the "day" diagram. *Journal of Geophysical Research: Solid Earth*, *123*(4), 2618-2644. doi: 10.1002/2017jb015247

Shah, J., Williams, W., Almeida, T. P., Nagy, L., Muxworthy, A. R., Kovács, A., … Dunin-Borkowski, R. E. (2018). The oldest magnetic record in our solar system identified using nanometric imaging and numerical modeling. *Nature Communications*, *9*(1), 1173. doi: 10.1038/s41467-018-03613-1

Stoner, E. C., & Wohlfarth, E. P. (1948). A mechanism of magnetic hysteresis in heterogeneous alloys. *Philosophical Transactions of the Royal Society of London. Series A, Mathematical and Physical Sciences*, *240*(826), 599-642. doi: 10.1098/rsta.1948.0007

Tauxe, L., Bertram, H. N., & Seberino, C. (2002). Physical interpretation of hysteresis loops: Micromagnetic modeling of fine particle magnetite. *Geochemistry Geophysics Geosystems*, *3*(10). doi: 10.1029/2001gc000241

Tauxe, L., Mullender, T. A. T., & Pick, T. (1996). Potbellies, wasp-waists, and superparamagnetism in magnetic hysteresis. *Journal of Geophysical Research: Solid Earth*, *101*(B1), 571-583. doi: 10.1029/95jb03041

Valdez-Grijalva, M. A., Muxworthy, A. R., Williams, W., Conbhuí, P. O., Nagy, L., Roberts, A. P., & Heslop, D. (2018). Magnetic vortex effects on first-order reversal curve (forc) diagrams for greigite dispersions. *Earth And Planetary Science Letters*, *501*, 103 – 111. doi: 10.1016/j.epsl.2018.08.027

Valdez-Grijalva, M. A., Nagy, L., Muxworthy, A. R., Williams, W., Roberts, A. P., & Heslop, D. (2020). Micromagnetic simulations of first-order reversal curve (forc) diagrams of framboidal greigite. *Geophysical Journal International*, *222*(2), 1126–1134. doi: 10.1093/gji/ggaa241

Williams, W., & Dunlop, D. J. (1990). Some effects of grain shape and varying external magnetic-fields on the magnetic-structure of small grains of magnetite. *Physics of the Earth and Planetary Interiors*, *65*(1-2), 1-14. doi: Doi10.1016/0031-9201(90)90070-E

Williams, W., & Dunlop, D. J. (1995). Simulation of magnetic hysteresis in pseudo-single-domain grains of magnetite. *Journal of Geophysical Research-Solid Earth*, *100*(B3), 3859-3871. doi: Doi10.1029/94jb02878

Williams, W., Fabian, K., P., R., Nagy, L., Paterson, G., & Muxworthy, A. R. (n.d.). *Merrill* [webpage]. Retrieved from `https://bitbucket.org/wynwilliams/merrill`

Zhao, G., Morvan, F., & Wan, X. (2014). Micromagnetic calculation for exchange-coupled nanocomposite permanent magnets. *Reviews in Nanoscience and Nanotechnology*, *3*(4), 227-258. doi: 10.1166/rnn.2014.1058